

Electric field gradients of $CeMIn_5$ ($M = Co, Rh, Ir$) heavy-fermion systems studied by perturbed angular correlations and *ab initio* electronic structure calculations

M. Forker,^{1,*} P. R. J. Silva,¹ J. T. P. D. Cavalcante,¹ F. H. M. Cavalcante,^{1,2} S. M. Ramos,¹ H. Saitovitch,¹ E. Baggio-Saitovitch,¹ R. Alonso,³ M. Taylor,³ and L. A. Errico^{3,4}

¹*Centro Brasileiro de Pesquisas Físicas - CBPF/MCTI; Rua Dr. Xavier Sigaud, 150; 22290-180, Rio de Janeiro, Brasil*

²*Instituto de Pesquisas Energéticas e Nucleares (IPEN/CNEN), São Paulo, Brasil*

³*Departamento de Física and Instituto de Física La Plata (IFLP, CONICET-UNLP), Facultad de Ciencias Exactas, Universidad Nacional de La Plata, CC 67, 1900 La Plata, Argentina*

⁴*Universidad Nacional del Noroeste de la Provincia de Buenos Aires (UNNOBA), Monteagudo 2772, Pergamino, CP 2700, Buenos Aires, Argentina*

(Received 16 January 2013; published 17 April 2013; corrected 22 April 2013)

The electric field gradient (EFG) at the highly dilute nuclear probe ^{111}Cd in the heavy fermion systems $CeMIn_5$, $M = Co, Rh$, and Ir and $YCoIn_5$ has been investigated by perturbed angular correlation (PAC) measurements of the nuclear electric quadrupole interaction (QI) of ^{111}Cd on In sites. Pure and Sn -doped single crystals prepared by In -flux synthesis and polycrystalline samples prepared by arc melting have been studied. The samples were doped with the PAC probe ^{111}Cd by diffusion of the mother isotope ^{111}In . In all samples, several fractions of ^{111}Cd probe nuclei subject to different QI's have been observed, among them a large fraction of ^{111}Cd in unreacted In metal. Detailed calculations of the EFG at In nuclei and at Cd probes on In sites of pure and Sn -doped $CeMIn_5$ were performed, using the full-potential augmented plane wave + local orbital (APW + lo) formalism and taking into account different variables such as the electronic structure of the hyperfine probes, probe induced structural distortions, and impurity doping. The excellent agreement between the predicted EFG's and the experimental results allows us to assign two of the observed EFG components to the lattice sites $1c$ and $4i$ of the $CeMIn_5$ compounds and to explain the pronounced difference of the EFG at In and Cd probes on the same lattice position. Structural distortions induced by the Cd probe and Sn -doping were found to have little effect on the EFG at the Cd probes. We also show that the local spin density approximation (LSDA) and $LDA + U$ calculations predict very similar equilibrium structures and EFG's at the In/Cd sites. The extension of the experiments and the calculations from $CeMIn_5$ to $YCoIn_5$ and $LaCoIn_5$ have established that the influence of the $4f$ electrons on the EFG's at impurity sites is negligibly small.

DOI: [10.1103/PhysRevB.87.155132](https://doi.org/10.1103/PhysRevB.87.155132)

PACS number(s): 71.15.-m, 71.27.+a, 76.60.Gv, 76.80.+y

I. INTRODUCTION

The Ce compounds $CeMIn_5$ ($M =$ group VIII transition metal), $YCoIn_5$, and $LaCoIn_5$ (generally referred to as the “115s” for their chemical composition) have received considerable attention in recent years because of their exceptional richness in low-temperature electronic phenomena, including heavy-fermion behavior and antiferromagnetic fluctuations together with unconventional superconductivity (see Ref. 1 and references therein).

Much of the experimental information presently available on $CeMIn_5$ with $M = Co, Rh$, or Ir has been obtained by measurements of hyperfine interactions (HFI) using nuclear quadrupole resonance (NQR) and nuclear magnetic resonance (NMR), mostly with ^{115}In and (to lesser extent) ^{59}Co as probe nuclei.¹⁻⁷

It has been established that the properties of the Ce -115 compounds can be modified by doping them with donor or acceptor impurities. The superconductivity of $CeCoIn_5$ is destroyed by substituting 3.6% of In by Sn ^{8,9} and hole doping by substitution of In by Cd allows reversible tuning between superconducting and antiferromagnetic ground states.^{10,11} The interaction between nuclear moments and extra-nuclear fields provides information on the charge and spin distributions in the close vicinity of the probe nuclei. Measurements of the electric and/or magnetic HFI of Sn or Cd impurities and the comparison with the HFI of the In constituents can

therefore possibly contribute to the understanding of the effect of these impurity states on the $CeMIn_5$ properties. Hyperfine interactions at Sn nuclei can be studied by ^{119}Sn Mössbauer spectroscopy and at Cd nuclei by $^{111}In \rightarrow ^{111}Cd$ perturbed angular correlations (PAC).¹²

To assess the potential and eventual difficulties of PAC spectroscopy for studies of the $CeMIn_5$ heavy-fermion systems, we have investigated the electric field gradient (EFG) at the Cd nuclei in $CeMIn_5$ by PAC measurements of the nuclear electric quadrupole interaction (QI) with the radio-isotope ^{111}Cd as probe nucleus. The EFG tensor is directly related to the anisotropy of the electronic density,¹² which in turn reflects the probe chemistry with its neighborhood.¹³

An important aspect of the present investigation concerns the sample preparation. Most studies of $CeMIn_5$ use single crystals synthesized by the In -flux technique.¹⁴ The 171–245 keV $\gamma\gamma$ -cascade of ^{111}Cd employed in PAC spectroscopy is populated by the electron capture decay of the 2.8 d isotope ^{111}In . The compounds to be investigated must therefore be doped with the radioisotope ^{111}In . As addition of radioactive ^{111}In to the In -flux synthesis is problematic for several reasons, the samples are better doped after synthesis, either by ion implantation or by diffusion. In the present case, diffusion was used to dope In -flux single crystals of the 115 family previously used in electrical resistivity measurements^{15,16} and polycrystalline samples prepared by arc-melting of the constituents.

As the $CeMIn_5$ structure contains two nonequivalent In sites (relative intensities 4:1, see below), the PAC spectra are expected to present at least two components with different QI parameters. The assignment of the experimental QI parameters to the In lattice sites, however, is not straightforward. The intensity ratio of the two PAC components must not necessarily agree with that of the lattice sites, since the sample preparation by diffusion might involve some site preference. Furthermore, since the probe nucleus ^{111}Cd is an impurity on In sites, an assignment based on the comparison of QI and lattice symmetry might also be problematic.

For these reasons, a reliable site assignment requires an accurate calculation of the EFG¹⁷ at the impurity sites in the system under study. This is possible through the use of an all-electron *ab initio* electronic structure calculation in the framework of the density-functional theory (DFT).¹⁸ By electronic structure calculations, the EFG's can be determined for different structural and electronic scenarios, which can then be compared to the experimental results. In this way, local properties such as the location of defects and impurities can be determined. Assignment of hyperfine interactions to structural sites was reported, for example, in Refs. 19 and 20.

In the present study, the full-potential linear augmented plane wave plus local orbital (APW+lo) method was used for the calculation. This method allows us to determine the electronic structure of pure and Cd-doped $CeMIn_5$ and the atomic relaxations introduced by the impurities in the host in a fully self-consistent way using a supercell approach. For an answer to the question to which extent the Ce-4*f* electrons affect the EFG (the key experimental quantity) at In and Cd sites, the calculations were extended to $YCoIn_5$ and $LaCoIn_5$.

This paper is organized as follows. In Sec. II, the systems under study are described. In Sec. III, we present the details of the sample preparation, the data analysis and our PAC results. In Sec. IV, we describe the method of calculation and the theoretical results. First, and to check the validity of our approach, we will briefly describe the results obtained in the pure systems. The results obtained for the structural properties are presented and compared to x-ray diffraction experiments. Our predictions for the EFG at In nuclei are compared with experimental NQR results and other calculations reported in the literature. We then present theoretical values for the EFG at Cd nuclei in various 115 compounds and, based on these calculations, we assign the experimentally determined hyperfine interactions to the 1*c* and 4*i* lattice positions of the $RMIn_5$ structure. The role of structural distortions and the influence of the Ce *f* electrons and of Sn dopants on the Cd-EFG are discussed. Finally, Sec. V contains the conclusions.

II. THE SYSTEMS UNDER STUDY

$CeMIn_5$ (and $LaCoIn_5$ and $YCoIn_5$) compounds are isostructural with the tetragonal $HoCoGa_5$ structure^{21–23} (space group $P4/mmm$, number 123). The structure consists of four atoms in the asymmetric unit cell where Ce, *M*, In1, and In2 atoms occupy the 1*a* ($4/mmm$), 1*b* ($4/mmm$), 1*c* ($4/mmm$), and 4*i* ($mm2$), sites, respectively. (For an illustration, see Fig. 1 of Ref. 1). The compounds $CeMIn_5$ (and similarly $LaCoIn_5$ and $YCoIn_5$) are built by monolayers of face-sharing distorted cuboctahedra ($CeIn_3$) and monolayers

TABLE I. Lattice parameters *a* and *c* and the positional parameter *z* for $CeCoIn_5$, $CeIrIn_5$, $CeRhIn_5$, $LaCoIn_5$, and $YCoIn_5$.

	$CeCoIn_5$ [Ref. 22]	$CeIrIn_5$ [Ref. 22]	$CeRhIn_5$ [Ref. 22]	$LaCoIn_5$ [Ref. 22]	$YCoIn_5$ [this work]
<i>a</i> (Å)	4.61292 ₉	4.674 ₁	4.656 ₂	4.6399 ₄	4.5094
<i>c</i> (Å)	7.5513 ₂	7.501 ₅	7.542 ₁	7.6151 ₆	7.4003
<i>z</i> (In-4 <i>i</i>)	0.3094 ₃	0.3052 ₂	0.3059 ₂	0.31134 ₉	0.3075

of edge-sharing rectangular parallelepipeds (MIn_2), stacked alternatively in the [001] direction. The key structural unit of the series is the distorted cuboctahedron ($CeIn_3$). Such a structural arrangement implies that the $CeMIn_5$ are quasi-2D variants of $CeIn_3$.²⁴ The positions of all the atoms in the unit cell are determined by one internal parameter *z*. Ce/La/Y atoms are located at (0,0,0), *M* at (0,0,1/2), In1 at (1/2,1/2,0), and In2 at (0,1/2,*z*). The cell constants and the positional parameter *z* of all the 115 compounds studied here are listed in Table I. As far as we know, no cell constants and the *z* parameter of $YCoIn_5$ were reported in the literature. For this reason, the equilibrium lattice parameters and positional parameter *z* in $YCoIn_5$ were calculated. For this purpose, we mapped the energy surface as a function of *a*, *c*, and *z* in order to obtain the lattice parameters corresponding to the minimum energy of the system (for details see Ref. 20). The results for the positional and the lattice parameters of $YCoIn_5$ are presented in Table I.

As the structure contains two nonequivalent In sites, two contributions to the PAC spectrum are expected, one from the axially symmetric 1*c* site located in the center of the basal plane close to four Ce atoms, and the other one from the lower symmetry 4*i* site surrounded by Ce and *M* ions.

III. EXPERIMENTS

A. Sample preparation

Compounds produced by two different routes of synthesis were studied. (i) A total of six 115-family single-crystal samples produced by the In-flux technique¹⁴ were investigated: Sn-doped single crystals $CeCo(In_{1-x}Sn_x)_5$ with $0.01 \leq x \leq 0.03$ (samples I, II, and VI in Table II), $CeRh(In_{1-x}Sn_x)_5$, $x = 0.032$ (sample III), nondoped $YCoIn_5$ (sample IV), and nondoped $CeCoIn_5$ (sample V). In the In-flux synthesis, stoichiometric amounts of Ce and Co are heated with In excess to 1423 K and subsequently cooled in a two-stage process rapidly to 1023 K and then slower to 723 K. At this temperature, the liquid In excess is removed with a centrifuge. (ii) A polycrystalline sample of nondoped $CeCoIn_5$ (sample VII in Table II) was produced by arc melting of stoichiometric quantities of the metallic constituents under argon atmosphere. An x-ray diffraction spectrum, taken after annealing in vacuum at 770 K for 7 days, confirmed the tetragonal $HoCoGa_5$ crystal structure of the sample. The intermediate state of the 171–245 keV PAC cascade of ^{111}Cd has a half-life of $T_{1/2} = 84$ ns; its spin is $I = 5/2$. To introduce the ($^{111}In \rightarrow$) ^{111}Cd probes into the samples, the mother isotope ^{111}In , commercially available as carrier-free aqueous solution of $^{111}InCl_3$, was deposited onto the samples,

TABLE II. Quadrupole interaction of the nuclear probe ^{111}Cd in five $CeIn_5$ -compounds: the relative intensity, the quadrupole frequency ν_q , the corresponding EFG component V_{zz} , and the asymmetry parameter η of the different components detected in the ^{111}Cd PAC spectra are listed. The results for several compounds, different routes of synthesis and diffusion temperatures T_{diff} are given. The assignment of components Cd2 and Cd3 to sites $1c$ and $4i$ of the $CeMIn_5$ structure is based on the *ab initio* calculation of the EFG described in Sec. IV, components Cd1 and Cd5 are identified by previous PAC measurements as ^{111}Cd on In sites of In metal²⁸ and $CeIn_3$,^{29,30} respectively. The low-frequency distribution of the polycrystalline sample (VII) is not listed. Question marks indicate uncertain assignments and/or unidentified components.

Compound	Sample number	Component-site assignment	Rel. intensity	$\nu_q = eQV_{zz}/h$ (Mhz)	V_{zz} (10^{21} V/m ²)	η
Group I: In flux synthesis						
$CeCo(In_{1-x}Sn_x)_5$ $x = 0.01, 0.03$ $T = 15$ K $T_{diff} = 670$ K Fig. 1	I, II	Cd 1 - In metal	0.42	26.6 ₁	1.43	0
		Cd 2 - $4i$?	0.36	245.8 ₃	13.85	0.658
		Cd 3 - $1c$	0.03	63.6 _{1,5}	3.41	0
		Cd 4 ?	0.18	321.1 ₃	17.24	0.0
$CeRh(In_{1-x}Sn_x)_5$ $x = 0.032$ $T = 15$ K $T_{diff} = 670$ K	III	Cd 1- In metal	0.42	29.1 ₂	1.56	0
		Cd 2 - $4i$	0.08	218.9 ₄	11.78	0.610 ₅
		Cd 6 ?	0.15 ₁	389.1 ₄	20.89	0.0
		Cd 7 ?	0.35 ₂	296.9 ₂	15.94	0.627 ₂
$YCoIn_5$ $T = 15$ K $T_{diff} = 670$ K	IV	Cd 1- In metal	0.64 ₂	25.3 ₁	1.36	0.00
		Cd 2 - $4i$	0.23 ₂	259.3	13.92	0.734
		Cd 4 ?	0.13 ₁	338.5 ₉	18.18	0.00
$CeCoIn_5$ $T = 15$ K, $T_{diff} = 770$ K Fig. 2	V	Cd 1 - In metal	0.32	23.9 ₂	1.28	0
		Cd 2 - $4i$	0.46	197.1 ₂	10.58	0.511
		Cd 3 - $1c$	0.15	65.5 ₅	3.51	0
		Cd 5 - $CeIn_3$	0.07	81.4 ₇	4.37	0
$CeCo(In_{1-x}Sn_x)_5$ $x = 0.025$ $T = 15$ K $T_{diff} = 770$ K	VI	Cd 1-In metal	0.53	24.2	1.29	0
		Cd 2 - $4i$	0.33	198.0 ₂	10.63	0.521
		Cd 3 - $1c$	0.08	64.4 ₅	3.46	0
		Cd 5 - $CeIn_3$	0.06	80.5 ₈	4.32	0
Group II: Arc melting						
$CeCoIn_5$ $T = 290$ K, $T_{diff} = 770$ K Fig. 4	VII	Cd 2 - $4i$	0.55	191.9 ₅	10.31	0.499 ₁
		Cd 3 - $1c$	0.18	66.5 ₃	3.57	0
		Cd 5 - $CeIn_3$	0.05	76.8 ₇	4.12	0
$LaCoIn_5$ $T = 290$ K	Ref. 31	$4i$	0.8	183.7	9.86	0.49
		$1c$	0.2	59.4	3.19	0

which were then encapsulated in vacuum and heated for 12 h to high temperatures. (Note: the mole fraction of $^{111}In/^{111}Cd$ probes in a standard PAC sample does not exceed about 10^{-8} .)

In the first single-crystal experiments (samples I–IV of Table II), the diffusion was carried out at 670 K (below the second cooling stage of the In-flux synthesis). The results of these measurements suggested that only part of the probe nuclei reached the In sites of the $CeCoIn_5$ structure. In later single-crystal experiments (samples V and VI) the diffusion temperature was raised to 770 K. The polycrystalline arc-melted sample (VII) was also doped at this temperature. X-ray diffraction spectra of $CeCoIn_5$ single crystals taken before and after heating to the diffusion temperature of 770 K for 12 h showed that the diffusion process leaves the $HoCoGa_5$ structure unchanged.

The PAC measurements were carried out with a standard four-detector BaF_2 setup in the temperature range 10 K $\leq T \leq 1073$ K. Temperatures $T < 290$ K were obtained with a closed-cycle He refrigerator, whereas temperatures $T > 290$ K were produced with an especially designed PAC furnace.²⁵

For the high-temperature measurements, the samples were encapsulated under vacuum into small quartz tubes.

B. Data analysis

The unperturbed angular correlation of a cascade of successive γ rays in nuclear decay can be expanded into a series of Legendre polynomials with the number k_{max} of (even) k depending on the spin I of the intermediate level and the multipolarities l of the γ transitions:¹²

$$W(\Theta) = \sum_{k=0}^{k_{max}} A_{kk} P_k(\cos \Theta), \quad k_{max} \leq \text{Min}(2I, 2l_1, 2l_2). \quad (1)$$

A hyperfine interaction in the intermediate state of the cascade leads to a time modulation of the $\gamma\gamma$ angular correlation. In the case of polycrystalline samples, this modulation can be expressed by a time-dependent perturbation factor:

$$W(\Theta) = \sum_{k=0}^{k_{max}} A_{kk} G_{kk}(t) P_k(\cos \Theta). \quad (2)$$

Here, we are dealing with static electric quadrupole interactions (QI) between the electric quadrupole moment Q of the intermediate state and the EFG acting at the nuclear site. The perturbation factor for a static QI can be written as¹²

$$G_{kk}(t) = \sum_0^n s_{kn} \cos(\omega_n t) \exp\left(-\frac{1}{2} \delta \omega_n t\right). \quad (3)$$

The hyperfine frequencies ω_n are related to the energy differences of the hyperfine levels into which the nuclear state is split by the QI. These frequencies depend on the quadrupole frequency

$$\nu_q = eQV_{zz}/h \quad (4)$$

and the asymmetry parameter

$$\eta = (V_{xx} - V_{yy})/V_{zz}, \quad (5)$$

where $V_{ii} = \delta^2 V / \delta i^2$; ($i = x, y, z$) are the principal-axis components of the EFG tensor with $|V_{xx}| \leq |V_{yy}| \leq |V_{zz}|$.

In polycrystalline samples, the amplitudes s_{kn} are functions of the asymmetry parameter η only. The number n of terms in Eq. (3) depends on the spin of the nuclear state under consideration. For $I = 5/2$, $n = 3$. The exponential factor accounts for possible distributions of the static QI caused by structural or chemical defects, which lead to an attenuation of the oscillatory PAC pattern. The parameter δ is the relative width of a Lorentzian distribution.

In the case of single-crystal samples, the perturbation depends—apart from the QI parameters ν_q and η —sensitively on the orientation (θ_i, φ_i) of the γ -ray detectors $i = 1, 2$ relative to the principal axes of the EFG tensor. By introducing effective amplitudes s_{kn}^{eff} , Wegner²⁶ has shown that for the present case of nuclear spin $I = 5/2$ the perturbation factor for QI's in single crystals can be brought to a form analogous to Eq. (3):

$$G_{kk}(t) = \sum_n s_{kn}^{\text{eff}} \cos(\omega_n t) \exp\left(-\frac{1}{2} \delta \omega_n t\right). \quad (6)$$

The effective amplitudes s_{kn}^{eff} depend on the asymmetry parameter, on the detector orientations (θ_i, φ_i) and the angular correlation coefficients.

When several fractions of nuclei subject to different hyperfine interactions are found in the same sample, the effective perturbation factor is given by

$$G_{kk}(t) = \sum_i f_i G_{kk}^i(t), \quad (7)$$

where f_i (with $\sum_i f_i = 1$) is the relative intensity of the i th fraction.

C. Experimental results

Figure 1 shows the PAC spectra of ^{111}Cd in $\text{CeCo}(\text{In}_{1-x}\text{Sn}_x)_5$, $x = 0.03$ (sample I), Fig. 2 those of nondoped CeCoIn_5 (sample V), both prepared by the In-flux technique. At $T \leq 290$ K (lower sections of Figs. 1 and 2), these spectra present fast oscillations of small amplitude superimposed on a relatively slow variation of the perturbation factor with time, indicating the presence of several fractions of ^{111}Cd probes subject to different QI's.

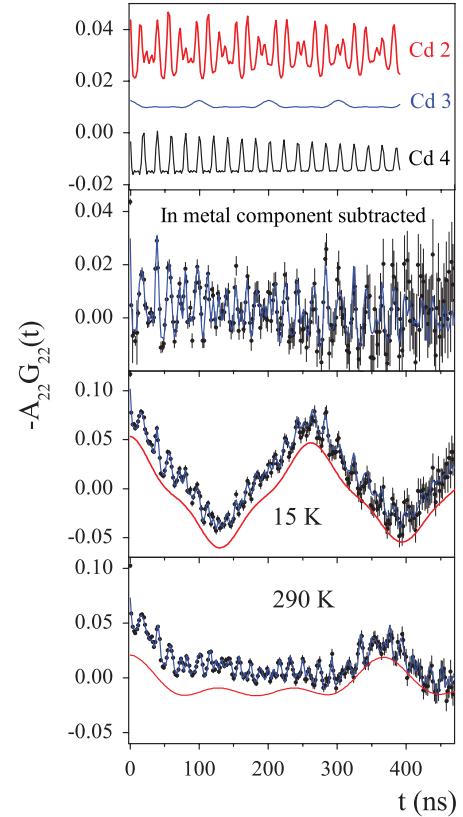


FIG. 1. (Color online) PAC spectra of ^{111}Cd in Sn-doped $\text{CeCo}(\text{In}_{1-x}\text{Sn}_x)_5$, $x = 0.03$ (sample I) at 290 and 15 K. The single-crystal sample, prepared by In-flux synthesis, was doped with $^{111}\text{In}/^{111}\text{Cd}$ by diffusion at 670 K. The spectrum contains four components: the dominant component Cd1 (red lines in the lower sections) shows that a large fraction of the probe nuclei reside in monocrystalline or strongly textured In-metal.

The spectra were analyzed by a least-squares fit of Eqs. (6) and (7) to the experimental data. The almost triangular form of the dominant fraction in the case of the 15 K-spectra of Figs. 1 and 2 is clear evidence for a monocrystalline or strongly textured sample. The amplitudes s_{kn}^{eff} of this fraction (red lines in the lower sections of Figs. 1 and 2) were therefore treated as adjustable parameters, whereas those of the other components were well described by the assumption of polycrystalline interactions. A total of four components or fractions were required for a satisfactory description of the measured spectra. Their relative intensities and the QI parameters ν_q and η at $T \geq 15$ K are listed in Table II.

The dominant fraction (termed component Cd1 in the following) that has been found in all 115 single crystals has axial symmetry $\eta = 0$ and a relative intensity of 35–65% (see Table II). In Fig. 3, the frequency of this component is plotted versus temperature on a $T^{3/2}$ scale²⁷ and compared to the temperature dependence of the quadrupole frequency of ^{111}Cd nuclei in In metal.²⁸ The perfect agreement in the temperature trends of In metal and of component Cd1 of $\text{CeCo}(\text{In}_{1-x}\text{Sn}_x)_5$; $x \leq 0.03$ is clear evidence for the presence of unreacted In metal in these 115 single-crystal samples. The slightly larger frequency in the case of $\text{CeRh}(\text{In}_{1-x}\text{Sn}_x)_5$ is possibly due to a

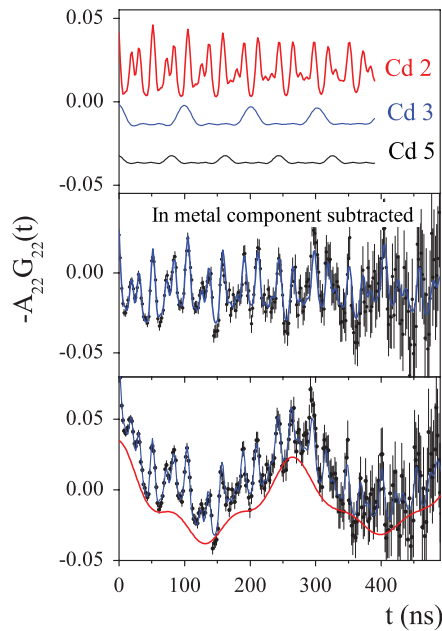


FIG. 2. (Color online) PAC spectrum of ^{111}Cd in pure CeCoIn_5 (sample V) at 15 K. The compound, synthesized by the In flux technique, was doped with the PAC probe $^{111}\text{In}/^{111}\text{Cd}$ by diffusion at 770 K. The analysis of the measured PAC spectrum (blue line in the bottom-most section) indicates the presence of several probe sites (Cd1–Cd5) with different QI parameters. The dominant contribution Cd1, represented by the red line in the bottom-most section, corresponds to ^{111}Cd probes in single-crystalline In metal. After subtraction of this In-metal component, the spectrum (middle section) contains three components denominated Cd2–Cd5, separated in the top-most section.

contamination of the In metal by constituent elements of the 115 crystals.

The conclusion that the In part of the samples is in a monocrystalline or at least in a strongly textured state is further supported by the pronounced change in the overall shape of

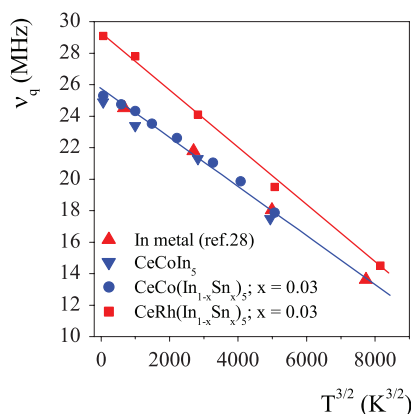


FIG. 3. (Color online) The quadrupole frequency of ^{111}Cd in pure In metal and of the component Cd1 of the ^{111}Cd PAC spectra of Ce-115-compounds grown by the In-flux technique vs temperature on a $T^{3/2}$ scale.

the Cd1 component between 15 and 295 K in Fig. 1: the 15 K spectrum was taken with the sample inside, that at 295 K with the sample outside the cryostat, and the orientation of the sample relative to the detector system has unintentionally been changed between the two measurements.

The fact that in contrast to the In metal component Cd1 the components Cd2–Cd7 are well described by the assumption of a polycrystalline interaction suggests that the In-flux samples contain several pieces of Ce-115 single crystals, randomly embedded in an environment of monocrystalline or strongly textured In metal.

The observation of a large In metal component indicates that the centrifuge separation of the In-flux is only partially successful. Obviously, considerable amounts of In metal still adhere to the Ce-115 crystals when they reach room temperature. When cooled from the diffusion temperature, the In excess solidifies and a strong texture forms.

The other components necessary to describe the PAC spectra are shown in the top-most section of Figs. 1 and 2. In pure (sample V, Fig. 2) and in Sn-doped (sample VI) CeCoIn_5 one finds the same components: one nonperiodic ($\eta \neq 0$; Cd2) and two periodic components ($\eta = 0$; Cd3, Cd5). As we will show in Sec. IV, Cd2 and Cd3 can be attributed to ^{111}Cd on sites 4i and 1c, respectively, of the HoCoGa_5 structure. From its QI parameters (ν_q, η), the second axially symmetric component (Cd5) can be identified as ^{111}Cd on the In site of the compound CeIn_3 .^{29,30}

Samples I and II [$\text{CeCo}(\text{In}_{1-x}\text{Sn}_x)_5$, $x = 0.01, 0.03$] are doped to about the same Sn concentration as sample VI. However, the quadrupole frequency of the component Cd2 of the latter sample is about 20 % smaller while the frequency of Cd3 is very similar in all the Sn-doped (samples I, II, VI) and non-Sn-doped (sample V) CeCoIn_5 compounds. Furthermore, samples I, II present a fast axially symmetric component Cd4 absent in samples V, VI.

The PAC spectrum of $^{111}\text{Cd}:\text{CeRh}(\text{In}_{1-x}\text{Sn}_x)_5$, $x = 0.032$ (sample III) contains one axially symmetric (Cd6) and two asymmetric (Cd2, Cd7) components. The PAC spectrum of YCoIn_5 (sample IV) showed the largest In metal component of all 115-family single crystals investigated ($\sim 65\%$). In addition to Cd1, two components were found: one ($\sim 23\%$) with an axially asymmetric QI ($\nu_q = 260$ MHz, $\eta = 0.73$), another one (12%) with a high frequency QI of axial symmetry ($\nu_q = 338$ MHz, $\eta = 0.0$) comparable to Cd4 in samples I and II and Cd6 in sample III.

The PAC spectra of polycrystalline CeCoIn_5 produced by arc melting of the constituents (sample VII, Fig. 4) are free of an In metal component. In this case, three components with sharp QI parameters are needed to describe the experimental data: Cd2 and Cd3 and component Cd5 identified as ^{111}Cd on the In site of the compound CeIn_3 .^{29,30} Furthermore, the slow decrease of the baseline of the 293-K spectrum in Fig. 4 suggests that a small fraction of the probe nuclei is subject to a low-frequency QI distribution similar to the one observed at 1073 K. The QI parameters of components Cd2 and Cd3 are very close to those found in the ^{111}Cd PAC study of LaCoIn_5 by Newhouse and Collins.³¹

For the polycrystalline compound and one nondoped single-crystal sample, the QI parameters of components Cd2 and Cd3 were studied as a function of temperature in the range

$4 \text{ K} \leq T \leq 1100 \text{ K}$. Weak temperature dependence was found:

$$d \ln v_q/dT|_{4\text{K}} = 1.22(3) \times 10^{-4} \text{ K}^{-1} \quad \text{for component Cd2 (site 4i),}$$

$$d \ln v_q/dT|_{4\text{K}} = 6.3(2.3) \times 10^{-5} \text{ K}^{-1} \quad \text{and} \quad d \ln \eta/dT|_{4\text{K}} = 6(2) \times 10^{-5} \text{ K}^{-1} \quad \text{for component Cd3 (site 1c).}$$

The high-temperature measurements also showed that the thermal stability of the 115 compounds studied here extends to about $T \sim 1000 \text{ K}$; only at higher temperatures the oscillatory structure of components Cd2 and Cd3 started to disappear.

IV. THEORY

A. Procedure

The analysis of the PAC spectra for diffused ($^{111}\text{In} \rightarrow$) ^{111}Cd impurities in the 115 compounds gave evidence for up to seven fractions, each with different EFG parameters, in the set of CeMIn_5 and YCoIn_5 samples. By comparison with the results of previous PAC studies on ^{111}In -doped in metallic In ²⁸ and in CeIn_3 ^{29,30} two of the fractions could be assigned to Cd substitutionally replacing In in metallic In and in CeIn_3 , respectively. The principal aim of the theoretical work was to

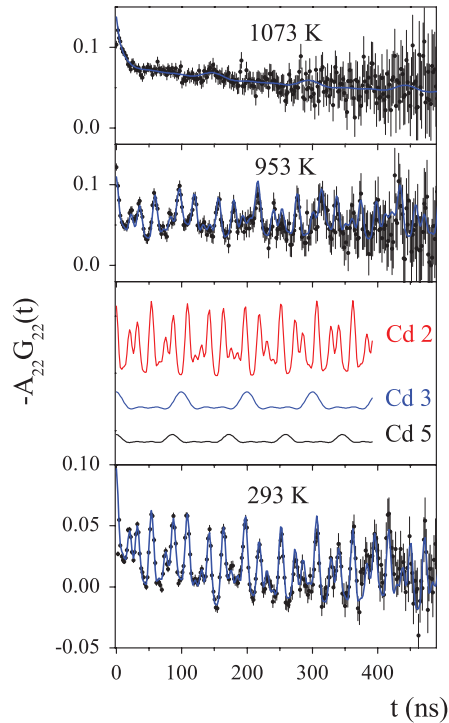


FIG. 4. (Color online) PAC spectra of ^{111}Cd in pure polycrystalline CeCoIn_5 (sample VII) at 295 K (bottom-most section). This sample was prepared by arc melting of the metallic constituents. After annealing at 700 K for 7 d, the compound was doped with the ^{111}In activity by diffusion at 770 K. Three components with sharp QI parameters are present: Cd2, Cd3 and Cd5. The slow decrease of the baseline of the 293-K spectrum reflects a low-frequency QI distribution similar to the one observed at 1073 K. Note that in contrast to the samples prepared by In-flux technique, the spectrum of the arc-melted compound contains no In metal component.

identify—among the five fractions left—the two components originating from sites 1c and 4i of the HoGaIn_5 structure. For this purpose, the EFG tensor at Cd impurities on these sites was calculated by *ab initio* electronic structure calculations for all compounds investigated. First, we determined the self-consistent potentials and charge densities inside the Cd-doped 115 hosts and then calculated the EFG tensor at a Cd probe nucleus replacing a single In atom on either sites 1c or 4i of the host lattice, taking into proper account the structural and electronic effects introduced by the impurities.

In order to simulate an isolated impurity, we employed the supercell (SC) method. The SC considered here consists of eight units cells of the 115 compounds repeated periodically, where one of the 40 In atoms is replaced by a Cd atom. This SC correspond to a system of composition $\text{CeM}(\text{In}_{1-x}\text{Cd}_x)_5$ with $x = 0.025$. The resulting 56-atoms SC (56A-SC) has dimensions $a' = 2a = b' = 2b$ and $c' = 2c$. Additional calculations were performed (for some selected cases) using SCs with 189 atoms ($a' = 3a = b' = 3b$ and $c' = 3c$). These additional calculations show that although a 2.5 at.% doping is large compared with parts per million (ppm) dilutions in the samples used in the PAC experiments, the choice of the 56A-SCs keeps the Cd atoms sufficiently far from each other (at least 9 Å) to avoid significant interactions. Thus, the 56-atoms SC is an excellent compromise between computational times and accuracy of the calculations.

DFT-based¹⁸ calculations have been performed with the APW+lo method³² as embodied in the WIEN2K code.³³ Exchange and correlation effects were treated using the local spin density approximation (LSDA)³⁴ and the Wu and Cohen (WC-GGA,³⁵) and the PBE-Sol parameterization of the general gradient approximation (GGA).³⁶ We also performed LDA+*U* calculations.³⁷ In this model, an additional on-site Coulomb interaction for the *f* states is introduced. It was verified that the results of these calculations do not change significantly upon variation of *U* between 2.7 and 10.0 eV. The EFG values listed in Table III were obtained with $U = 8.1 \text{ eV}$, a value typical for the lanthanides. The parameter RK_{max} , which controls the size of the basis set, was fixed to 8.0 for the pure systems. In the case of the 56 atoms-SC we used $RK_{\text{max}} = 7.0$ (R is the smallest muffin tin radius and K_{max} the largest wavenumber of the basis set). Integration in the reciprocal space was performed using the tetrahedron method taking up to 5000 k points in the first Brillouin zone for the pure systems and 500 k points for the 56-atom SC's. Atomic displacements around the impurity have been obtained in the standard way described elsewhere (see^{38,39}). In all cases the lattice parameters were fixed to the experimental values (with the exception of YCoIn_5 , see Sec. II) and only the internal atomic positions were minimized. The diagonal elements of the EFG tensor were obtained directly from the V_{2M} components of the lattice harmonic expansion of the self-consistent potential.⁴⁰ The largest component V_{zz} of the diagonalized EFG tensor is

TABLE III. The electric field gradient (EFG) at In sites/nuclei in nondoped $RMIn_5$; $R = Ce, Y, La$ and $M = Co, Rh, Ir$. Theoretical results of the positional parameter z , the largest component V_{zz} of the diagonalized EFG tensor, and the asymmetry parameter η obtained with the procedures of the present study as described in Sec. IV A and some theoretical results by other authors are compared to experimental values. The experimental EFG's were derived from the measured quadrupole frequencies using $Q(^{115}In; 9/2) = 0.77$ b.⁴¹ In the case of the LDA + U calculations $U = 8.2$ eV was used. V_{zz} values are in units of 10^{21} V/m². For sites In-1c, one has $\eta = 0.00$.

Compound	Procedure	Positional parameter	EFG site 1c	EFG site 4i	
		z	V_{zz}	V_{zz}	η
CeCoIn ₅	LDA	0.3094	11.3	20.5	0.27
	WC-GGA	0.3089	10.9	19.7	0.29
	PBE-sol	0.3089	10.9	19.7	0.29
	LDA + U	0.3091	9.9	19.2	0.30
	Theor. Ref. 1		10.09	19.2	0.37
	Theor. Ref. 43		12.63	20.1	0.28
	Experiment	0.3094 ₃ Ref. 22	10.53	19.96	0.39
CeRhIn ₅	LDA	0.3037	10.3	21.4	0.35
	WC-GGA	0.3031	10.0	20.8	0.36
	PBE-sol	0.3031	9.9	20.7	0.37
	LDA + U	0.3030	9.9	19.9	0.36
	Theor. Ref. 1		7.94	21.4	0.43
	Experiment	0.3059 ₂ Ref. 22	8.73	21.48	0.45
CeIrIn ₅	LDA	0.3031	9.5	22.8	0.35
	WC-GGA	0.3018	9.2	22.2	0.35
	PBE-sol	0.3018	9.1	22.2	0.36
	LDA + U	0.3016	8.0	19.8	0.37
	Experiment	0.3052 ₂ Ref. 22	7.81	23.42	0.46
				Ref. 3 and 4	
YCoIn ₅	LDA	0.3088	10.0	18.7	0.38
	WC-GGA	0.3080	9.8	18.2	0.39
	PBE-sol	0.3078	9.7	18.1	0.39
LaCoIn ₅	LDA	0.3133	10.5	20.1	0.28
	WC-GGA	0.3119	9.9	19.4	0.33
	PBE-sol	0.3120	9.9	19.4	0.34
	Experiment	0.31134 ₉ Ref. 23	–	–	–

related to the experimentally determined quadrupole coupling constant ν_q by Eq. (4). The quadrupole moments Q of the $I = 9/2^+$ ground state of ^{115}In and of the $I = 5/2$ 482 KeV excited state of ^{111}Cd are $Q(^{115}In) = +0.774$ b,⁴¹ and $Q(^{111}Cd) = +0.773$ b,⁴², respectively.

The precision of the present results was checked by several additional calculations. For selected systems, the basis set (number of plane waves), the number of k points was increased and the effect of the muffin-tin radii on the relevant electronic and structural properties was studied. For the parameters previously detailed values of the EFG's and the interatomic distances can be obtained with adequate precision (the interatomic distances and the EFG components are converged to less than 0.01 Å and 0.1×10^{21} V/m², respectively). The procedure outlined here has been used to calculate the EFG at the In sites of pure 115 compounds, the EFG at Cd nuclei on In sites of $RM(In_{1-x}Cd_x)_5$ and to study the influence of the Ce-4*f* electrons on the EFG at Cd sites.

B. Theoretical results: EFG at Cd nuclei on In sites of $RM(In_{1-x}Cd_x)_5$, $x = 0.025$; $R = Ce, Y, La$ and $M = Co, Ir, Rh$.

The EFG at In nuclei in pure Ce115 compounds has been measured with high accuracy by ^{115}In NQR spectroscopy.^{1,3-6,43} The comparison with the present PAC results for ^{111}Cd shows that the EFG at Cd nuclei on sites 4*i* and 1c is much weaker than that at In nuclei on the same lattice positions (see Tables III and IV). For an understanding of these differences, we have calculated not only the Cd-EFG in doped $CeM(In_{1-x}Cd_x)_5$ compounds, but also the In-EFG for various pure 115 systems.

The theoretical positional parameters z and the EFG parameters V_{zz} , η at In nuclei in pure 115 compounds are listed in Table III. It can be seen that the results obtained using LDA, WC-GGA, PBE-sol, and LDA + U are very similar and are in very good agreement with the experimental results reported in the literature.^{3-6,22,23} In Table III we also present our results for V_{zz} and η at sites 1c and 4*i* for the three

TABLE IV. Theoretical (LDA) and experimental EFG parameters V_{zz} and η of In nuclei on sites $1c$ and $4i$ of nondoped $R\text{MIn}_5$ ($R = \text{Ce}, \text{Y}, \text{La}$; $M = \text{Co}, \text{Rh}, \text{Ir}$) and of Cd nuclei on the same lattice positions of the corresponding Cd-doped compounds $R\text{M}(\text{In}_{1-x}\text{Cd}_x)_5$; $x = 0.025$. For Cd nuclei, the theoretical EFG parameters V_{zz} and η are given for unrelaxed and equilibrium-relaxed structures. The experimental EFG parameters of the In nuclei are taken from Refs. 3,4, and 6, those of ^{111}Cd in LaCoIn_5 from Ref. 31. V_{zz} values are in units of 10^{21} V/m^2 .

Compound	Site	In nuclei on sites $1c, 4i$				Cd nuclei on sites $1c, 4i$					
		Theory		Experiment		Theory unrelaxed		Theory relaxed		Experiment	
		V_{zz}	η	V_{zz}	η	V_{zz}	η	V_{zz}	η	V_{zz}	η
CeCoIn ₅	$1c$	11.3	0	10.5	0	4.3	0	4.3	0	3.4	0
	$4i$	20.5	0.27	19.9	0.386	12.7	0.50	12.7	0.51	10.22	0.511
CeRhIn ₅	$1c$	10.3	0	8.7	0	4.4	0	4.1	0	–	–
	$4i$	21.4	0.35	21.5	0.445	13.6	0.59	13.2	0.49	11.8	0.61
CeIrIn ₅	$1c$	9.5	0	7.8	0	4.1	0	3.8	0	–	–
	$4i$	22.8	0.35	23.4	0.462	14.0	0.49	14.6	0.58	–	–
YCoIn ₅	$1c$	10.1	0	–	–	5.1	0	4.5	0	–	–
	$4i$	18.8	0.38	–	–	12.3	0.56	11.6	0.45	13.9	0.734
LaCoIn ₅	$1c$	10.5	0	–	–	4.8	0	4.2	0	3.2	0
	$4i$	20.1	0.28	–	–	13.1	0.49	12.5	0.42	9.9	0.49

models employed for the exchange and correlation potentials. The calculated EFGs show only a weak dependence on the selected exchange-correlation potential, giving systematically a smaller value for the GGA parameterizations. The difference between LDA + U (localized Ce- f electrons model) and LDA and both GGA parameterizations (delocalized models) is larger: LDA + U predicts a reduction of about 10–15% (depending on the compound considered) of V_{zz} in the case of site $1c$ compared to LDA and both GGA parameterizations. In the case of site $4i$, the localization of the Ce f -states produces a small reduction of about 2% when compared to the LDA, WC-GGA, and PBE-sol. Similar results were found in Ref. 1 where different delocalized and localized models were employed to describe the Ce- $4f$ electrons.

To calculate the EFG at Cd impurities localized at the two In sites of the 115 structures, we have replaced one In atom on site $1c$ or site $4i$, respectively, by a Cd atom in the supercell as described in Sec. II. Due to the larger computational cost, we performed mainly LDA calculations, but for some selected systems we also performed calculations using WC-GGA, PBE-sol, and LDA + U . From these tests, it was found that the EFG differences predicted by the four models employed for the correlation and exchange potential are similar to those found in the case of the pure systems.

The substitution of In atoms by Cd produces non-negligible forces on its nearest neighbors. Since even small changes in the atomic positions can induce large effects on the EFG and even more on the asymmetry parameter, full relaxation of all atomic positions were considered, until forces on the atoms were below 0.01 eV/\AA . We used this tolerance criterion because the changes in the EFG components induced by weaker forces are below the convergence error. The magnitudes of the structural distortions introduced by the Cd impurity were found to be very small (displacements smaller than 0.06 \AA).

The effect of the relaxation on the EFG at the impurity site is illustrated in Table IV, where we compare the Cd-EFG's of the unrelaxed structure (all atoms in the positions of the pure compounds) and that of the equilibrium-relaxed structure. It

can be seen that the changes of the EFG produced by the relaxation process are relatively small (below 10%). Table IV also compares the theoretical EFG values of In and Cd probes on sites $4i$ and $1c$ for different 115 compounds and lists the experimental values available for both probes.

The comparison between the theoretical EFG parameters of Cd impurities sites $4i$ and $1c$ in Table IV and the experimental EFG values in Table II clearly allows assigning the PAC components Cd2 and Cd3 to sites $4i$ and $1c$, respectively, of the 115 structure, as put forward in Tables II and IV.

It is interesting to note the large differences in the EFG parameters of indigenous In and impurity Cd nuclei on the same lattice positions of the 115 structure: for the axially symmetric site $1c$, the magnitude of the Cd-EFG is about a factor of 2 smaller than the In-EFG, for site $4i$ the magnitudes differ by about 80% and the asymmetry of the Cd-EFG is systematically larger.

To relate these observations to differences in the electronic structures of In and Cd, the partial charges in the In and Cd muffin-tin spheres were calculated. For simplicity, only the results obtained for CeCoIn₅ are presented here (a very similar behaviour was found in the case of the other 115 compounds investigated). It can be seen in Table V that the populations of the s , p , and d states of In are $0.14e$, $0.15e$, and $0.2e$ larger than those of Cd.

To discuss the effect of the different population on the EFG, it is sufficient to consider the valence contribution to the EFG, which originates from the nonspherical electron density of the valence and semicore electrons within the muffin-tin sphere of the probe nucleus.⁴⁰ In the present cases, the lattice term (originating from more distant regions of the crystal) is almost negligible (see Table V). The dominant valence contribution can be further decomposed according to the different orbital symmetries.⁴⁴ From this decomposition, we found that the In- $5p$ (Cd- $5p$) contribution to the EFG at the In (Cd) probes largely exceeds the d contribution, with the s contribution being almost negligible. From this decomposition, we identify the 0.15 additional electron with

TABLE V. Orbital populations (in electrons) and total, valence and s , p , and d valence contributions to the electric-field gradient (in units of 10^{21} V/m²) at In nuclei in nondoped $CeCoIn_5$ and at Cd nuclei in Cd-doped $CeCo(In_{1-x}Cd_x)_5$.

	Orbital populations							
	Partial charges at In nuclei		Partial charges at Cd nuclei					
	Site 1c	Site 4i	Site 1c	Site 4i				
s	0.77	0.76	0.63	0.62				
p	0.49	0.50	0.34	0.35				
d	9.68	9.69	9.48	9.48				
	Electric field gradients							
	In on site 1c		In on site 4i		Cd on site 1c		Cd on site 4i	
	V_{zz}	V_{zz}	η	V_{zz}	V_{zz}	η		
Total	11.5	20.44	0.27	4.3	12.73			
valence	11.54	20.46	0.27	4.32	12.52			
s	-0.06	-0.1	0.4	-0.02	-0.1			
p	12.28	21.01	0.25	5.3	14.0			
d	-0.70	-0.45	0.87	-1.0	-1.4			
experiment	10.6	20.2	0.39	3.4	10.22	0.51		

p character of In as responsible for the large difference of the In- and Cd-EFG's.

To estimate a possible contribution of the Ce-4*f* electrons to the EFG at the Cd sites, we have replaced the Ce constituents of the relaxed structure of $CeCo(In_{1-x}Cd_x)_5$, $CeRh(In_{1-x}Cd_x)_5$, and $CeIr(In_{1-x}Cd_x)_5$ by La atoms with fixed atomic positions and calculated the EFG for Cd on sites 1*c* and 4*i*. No significant changes ($\leq 2\%$) of the Cd-EFG were obtained, indicating that the EFG at the Cd sites is “short-sighted” to the type of neighbours (Ce or La), and, in consequence, to the 4*f* electrons of Ce.

The same holds for the effect of the Sn contamination on the EFG at Cd sites of $CeCo(In_{1-x}Cd_x)_5$. Replacing one of the first In neighbors of Cd on sites 1*c* or 4*i* by a Sn atom (distances Cd-Sn of the order of 3.3 Å) and accounting in a new relaxation process for the structural distortions introduced by the Sn dopants changes the EFG tensor components by about 0.1×10^{21} V/m². This theoretical result is in agreement with the experimental observation of identical ¹¹¹Cd quadrupole frequencies in $CeCo(In_{1-x}Sn_x)_5$ and $CeCoIn_5$ (samples V and VI in Table II).

V. DISCUSSION AND CONCLUSIONS

The measurement of hyperfine parameters as the EFG by NMR and PAC can provide detailed information on structural and electronic properties of the system under study. In the present case, impurity states in $CeMIn_5$ are studied by comparing the EFG's at Cd impurities to the EFG's at the In constituents. The interpretation of such measurements is not straightforward and situations may occur where different hyperfine interactions must be assigned to different lattice sites. In the case of impurity probes, arguments based on symmetry considerations may fail, since the chemical nature of the impurity may—through structural and/or electronic distortions of its neighbourhood—strongly affect the EFG. To unravel these complex cases, a realistic theory that

models different structural and electronic scenarios is of great help.

The present work concerns such complex systems, namely $CeMIn_5$, $YCoIn_5$, and $LaCoIn_5$ doped with low concentrations ($\leq 10^{-8}$) of the PAC probes ¹¹¹In \rightarrow ¹¹¹Cd. In principle, the impurity probe atoms can populate two different crystallographic sites in these compounds. PAC revealed (depending on the system considered and the sample preparation) up to four EFG components. To assign these hyperfine interactions to the crystallographic sites, DFT calculations of electronic structure have been used to describe $CeMIn_5$, $YCoIn_5$, and $LaCoIn_5$ in their pure forms as well as with substitutional Cd impurity probes.

In Table II, the QI parameters of the samples investigated are grouped according to the synthesis conditions. According to these data, samples V, VI (In flux), and VII (arc melting) present similar ¹¹¹Cd QI parameters; apart from the large In metal component of the In-flux single crystals (and a small contamination by $CeIn_3$ in some cases), one observes two components: one component characterized by the low-temperature parameters $\nu_q = 198_1$ MHz corresponding to $V_{zz} = 10.6 \times 10^{21}$ V/m², $\eta = 0.51_1$, the other one by $\nu_q = 65_1$ MHz corresponding to $V_{zz} = 3.5 \times 10^{21}$ V/m², $\eta = 0.00$. As suggested by the asymmetry parameters and confirmed by the *ab initio* calculations, the first component corresponds to ¹¹¹Cd on In-4*i* sites the second one to ¹¹¹Cd on In-1*c* sites of the 115 structures. The *ab initio* calculations furthermore explain that the substantial difference of the EFG values of the Cd impurities and of the In constituents on the same lattice sites is a consequence of the larger 5*p* electron population at the In probes.

Sn substituting In up to a concentration of 2.5% leaves these values unchanged. In the Sn-doped single-crystal and the arc-melted samples, the relative intensity of the interaction associated to the In-1*c* site corresponds to the theoretical value of 20%. In the nondoped single crystals (sample V) a considerable deviation from the theoretical expectation was found (see Table II).

The QI parameters of samples I–IV differ substantially from those of samples V–VII. Frequency and asymmetry of the interaction associated to the asymmetric site $4i$ are significantly larger. Site $1c$ ($\nu_q \sim 65$ MHz, $\eta = 0.00$) is observed with a reduced relative intensity of 10 percent only in $\text{CeCo}(\text{In}_{1-x}\text{Sn}_x)_5$ (samples I and II). In the other compounds, site $1c$ is completely missing, but all show a sizeable high-frequency ($\nu_q > 300$ MHz, $V_{zz} > 16 \times 10^{21}$ V/m²) axially symmetric component absent in samples V–VII. The reasons for these differences in the $4i$ QI parameters and the origin of the strong 300-MHz component are open questions. Admixtures of intermetallic phases of the Ce–In, Ce–Sn, Co–In, and Co–Sn systems might be considered. Among the compounds investigated up to now by ^{111}Cd PAC spectroscopy^{29,45–47} only the quadrupole frequencies of $^{111}\text{Cd}:\text{CoSn}$ ⁴⁶ come relatively close to 300 MHz; however, the interactions are axially asymmetric ($\eta \neq 0$). Co–In compounds have yet to be studied by PAC.

One might speculate that the differences in the $4i$ QI parameters and the appearance of unexpected components of samples I–IV relative to samples V–VII are a consequence of the higher diffusion temperature ($T_{\text{diff}} = 770$ K for samples V–VII versus $T_{\text{diff}} = 670$ K for samples I–IV). Accidental variations in the quality of the In-flux samples (contaminations by other phases, etc.) are another possible explanation. For a conclusion, a systematic study of a larger number of Ce₁₁₅ single crystals would be necessary.

As a final comment on the experimental part, we point out that this investigation provides the basis for further PAC studies of CeMIn_5 or related systems. The study of the spin polarization by measurement of the magnetic hyperfine field at ^{111}Cd in the antiferromagnetic phase of $\text{CeCo}(\text{In}_{1-x}\text{Cd}_x)_5$ appears particularly interesting. However, the present data have shown that the diffusion of the probe atoms into single crystal samples synthesized by the In flux technique leads to a number of problems for hyperfine interactions studies of CeMIn_5 and other In-containing heavy fermion systems by PAC spectroscopy. The most serious one is the In metal component in the PAC spectra of all single-crystal samples. The large relative intensity of this component does not necessarily imply that the samples actually contain 50% or more of unreacted In metal since diffusing ^{111}In might show a pronounced preference for In metal over the In sites of CeMIn_5 . A large In metal component in the PAC spectra, however, reduces the accuracy of the relevant CeMIn_5 components and less intense components might even escape detection. The appearance of components of uncertain origin leads to further difficulties for the interpretation of the PAC spectra of In-flux single crystals. For future PAC studies of hyperfine interactions in CeMIn_5 or related systems, polycrystalline arc-melted samples therefore

appear to be the better choice as long as the orientation of the EFG tensor or that of the magnetic hyperfine field in the antiferromagnetic phase relative to the crystal axes are not of central interest.

The theoretical part of the present study was motivated by two issues. First, there was the need to identify among the various QI parameters detected in the PAC spectra those corresponding to ^{111}Cd on In sites $1c$ and $4i$ of CeMIn_5 . Second, there is the observation of a large difference in the EFG's of the nuclear probes ^{115}In (NQR) and ^{111}Cd (PAC) on the same lattice sites and the question of the changes in the local electronic structure responsible for this difference. We therefore performed an APW + l_0 study of structural and electronic properties of pure and Cd-doped CeMIn_5 compounds. The equilibrium structure and the EFG's at In constituents and at Cd impurities on In sites were calculated using the LSDA and LDA + U approximations for the exchange and correlation potential. Both approximations predict very similar equilibrium structures and very nicely reproduce the experimental EFG's at the probe nuclei ^{115}In and ^{111}Cd . Apart from identifying the QI parameters of ^{111}Cd on sites $1c$ and $4i$, the calculations indicate that the large difference between the In- and the Cd-EFG is the consequence of a larger $5p$ electron population at the In site. Furthermore, the calculations show that the structural distortions induced by the Cd impurity have little effect on the EFG and that the influence of the $4f$ electrons and of Sn doping on the EFGs at Cd sites is negligibly small. To conclude, these results confirm the important role of LDA calculations not only for site identification in multi-site compounds, but also as a powerful tool for local structure studies.

ACKNOWLEDGMENTS

M.F. gratefully acknowledges the kind hospitality extended to him at CBPF and the financial support as Bolsista CAPES/Brasil. F.H.M.C. acknowledges financial support as Bolsista CNPq and FAPESP, Brazil. This work was partially supported by UNNOBA, Consejo Nacional de Investigaciones Científicas y Técnicas (CONICET) under Grant PIP0002. This research made use of the HP-Parallel-Computing Bose Cluster, the computational facilities at IFLP and Departamento de Física (UNLP) and the Huge Computing Cluster, Department of Physics and Astronomy, Aarhus University, DK-8000 Aarhus C, Denmark. The In-flux single crystals were provided by the group of P. G. Pagliuso at UNICAMP, São Paulo, Brazil. Furthermore, the authors are grateful to the radiochemistry department of IPEN/CNEN, São Paulo, Brazil for providing the ^{111}In radioactivity.

*Corresponding author: forker@hiskp.uni-bonn.de

¹J. Ruzs, P. M. Oppeneer, N. J. Curro, R. R. Urbano, Ben-Li Young, S. Lebègue, P. G. Pagliuso, L. D. Pham, E. D. Bauer, J. L. Sarrao, and Z. Fisk, *Phys. Rev. B* **77**, 245124 (2008).

²N. J. Curro, *New J. Phys.* **8**, 173 (2006).

³Y. Kohori, Y. Yamato, Y. Iwamoto, T. Kohara, E. D. Bauer, M. B. Maple, and J. L. Sarrao, *Phys. Rev. B* **64**, 134526 (2001).

⁴G.-Q. Zheng, K. Tanabe, T. Mito, S. Kawasaki, Y. Kitaoka, D. Aoki, Y. Haga, and Y. Onuki, *Phys. Rev. Lett.* **86**, 4664 (2001).

⁵N. J. Curro, P. C. Hammel, P. G. Pagliuso, J. L. Sarrao, J. D. Thompson, and Z. Fisk, *Phys. Rev. B* **62**, R6100 (2000).

⁶N. J. Curro, B. Simovic, P. C. Hammel, P. G. Pagliuso, J. L. Sarrao, J. D. Thompson, and G. B. Martins, *Phys. Rev. B* **64**, R180514 (2001).

- ⁷M. Yashima, S. Taniguchi, N. Tagami, Y. Mugino, H. Mukuda, Y. Kitaoka, Y. Ota, H. Shishido, R. Settai, and Y. Onuki, *Physica C* **470**, 558 (2010).
- ⁸E. D. Bauer, N. O. Moreno, D. J. Mixson, J. L. Sarrao, J. D. Thompson, M. F. Hundley, R. Movshovich, and P. G. Pagliuso, *Physica B (Amsterdam)* **359-361**, 35 (2005).
- ⁹M. Daniel, E. D. Bauer, S.-W. Han, C. H. Booth, A. L. Cornelius, P. G. Pagliuso, and J. L. Sarrao, *Phys. Rev. Lett.* **95**, 016406 (2005).
- ¹⁰L. D. Pham, Tuson Park, S. Maquilon, J. D. Thompson, and Z. Fisk, *Phys. Rev. Lett.* **97**, 056404 (2006).
- ¹¹R. R. Urbano, B.-L. Young, N. J. Curro, J. D. Thompson, L. D. Pham, and Z. Fisk, *Phys. Rev. Lett.* **99**, 146402 (2007).
- ¹²E. N. Kaufmann and R. J. Vianden, *Rev. Mod. Phys.* **51**, 161 (1979); H. Frauenfelder and R. M. Steffen, in *Alpha-, Beta-, and Gamma-Ray Spectroscopy*, edited by K. Siegbahn (North Holland, Amsterdam, 1966), Vol. 2; A. Lerf and T. Butz, *Angew. Chem., Int. Ed. Engl.* **26**, 110 (1987); G. Schatz and A. Weidinger, in *Nuclear Condensed Matter Physics: Nuclear Methods and Applications* (Wiley, Chichester, England, 1996); G. L. Catchen, *MRS Bull.* **20**, 37 (1995).
- ¹³S. Cottenier, V. Bellini, M. Çakmak, F. Manghi, and M. Rots, *Phys. Rev. B* **70**, 155418 (2004), and references therein.
- ¹⁴C. Petrovic, R. Movshovich, M. Jaime, P. G. Pagliuso, M. F. Hundley, J. L. Sarrao, Z. Fisk, and J. D. Thompson, *Europhys. Lett.* **53**, 354 (2001).
- ¹⁵S. M. Ramos, M. B. Fontes, A. D. Alvareng, E. Baggio-Saitovitch, P. G. Pagliuso, E. D. Bauer, J. D. Thompson, L. Sarrao, and M. A. Continentino, *Physica B* **359-361**, 398 (2005).
- ¹⁶S. M. Ramos, M. B. Fontes, E. N. Hering, M. A. Continentino, E. Baggio-Saitovich, F. D. Neto, E. M. Bittar, P. G. Pagliuso, E. D. Bauer, J. L. Sarrao, and J. D. Thompson, *Phys. Rev. Lett.* **105**, 126401 (2010).
- ¹⁷H. Akai, M. Akai, S. Blügel, B. Drittler, H. Ebert, K. Terakura, R. Zeller, and P. H. Dederichs, *Prog. Theor. Phys. Suppl.* **101**, 11 (1990).
- ¹⁸P. Hohenberg and W. Kohn, *Phys. Rev.* **136**, B864 (1964); W. Kohn and L. J. Sham, *ibid.* **140**, A1133 (1965).
- ¹⁹L. A. Errico, M. Rentería, and H. M. Petrilli, *Phys. Rev. B* **75**, 155209 (2007).
- ²⁰L. A. Errico, H. M. Petrilli, L. A. Terrazos, A. Kulińska, P. Wodniecki, K. P. Lieb, M. Uhrmacher, J. Belosevic-Cavor, and V. Koteski, *J. Phys.: Condens. Matter* **22**, 215501 (2010).
- ²¹Y. N. Grin, Y. P. Yarmolyuk, and E. I. Gladyshevskii, *Sov. Phys. Crystallogr.* **24**, 137 (1979).
- ²²E. G. Moshopoulou, J. L. Sarrao, P. G. Pagliuso, N. O. Moreno, J. D. Thompson, Z. Fisk, and R. M. Ibberson, *Appl. Phys. A* **74**, S895 (2002).
- ²³R. T. Macaluso, J. L. Sarrao, P. G. Pagliuso, N. O. Moreno, R. G. Goodrich, D. A. Browne, F. R. Fronczek, and J. Y. Chan, *J. Solid State Chem.* **166**, 245 (2002).
- ²⁴N. D. Mathur, F. M. Grosche, S. R. Julian, I. R. Walker, D. M. Freye, R. K. W. Haselwimmer, and G. G. Lonzarich, *Nature (London)* **394**, 39 (1998).
- ²⁵M. Forker, W. Herz, U. Hütten, M. Müller, R. Müßeler, J. Schmidberger, D. Simon, A. Weingarten, and S. C. Bedi, *Nucl. Instrum. Methods Phys. Res., Sect. A* **327**, 456 (1993).
- ²⁶D. Wegner, *Hyperfine Interact.* **23**, 197 (1985).
- ²⁷U. Köbler, *J. Phys.: Condens. Matter* **14**, 8861 (2002), and references therein.
- ²⁸E. Bodenstedt, U. Ortabasi, and W. H. Ellis, *Phys. Rev. B* **6**, 2909 (1972).
- ²⁹G. Schwartz and D. Shirley, *Hyperfine Interact.* **3**, 67 (1977).
- ³⁰A. W. Carbonari, J. Mestnik-Filho, R. N. Saxena, and H. Saitovitch, *Hyperfine Interact.* **133**, 77 (2001).
- ³¹R. Newhouse and G. S. Collins, [arXiv:1109.2262](https://arxiv.org/abs/1109.2262).
- ³²E. Sjöstedt, L. Nordström, and D. J. Singh, *Solid State Commun.* **114**, 15 (2000); G. K. H. Madsen, P. Blaha, K. Schwarz, E. Sjöstedt, and L. Nordström, *Phys. Rev. B* **64**, 195134 (2001); see also S. Cottenier, *Density Functional Theory and the Family of (L)APW- Methods: A Step-by-Step Introduction* (KU Leuven, Belgium, 2002) (http://www.wien2k.at/reg_user/textbooks).
- ³³P. Blaha, K. Schwarz, G. Madsen, D. Kvasnicka, and J. Luitz, *WIEN2k, An Augmented Plane Wave Plus Local Orbitals Program for Calculating Crystal Properties* (Karlheinz Schwarz, Technical Universität Wien, Austria, 1999).
- ³⁴J. P. Perdew and Y. Wang, *Phys. Rev. B* **45**, 13244 (1992).
- ³⁵Z. Wu and R. E. Cohen, *Phys. Rev. B* **73**, 235116 (2006).
- ³⁶J. P. Perdew, A. Ruzsinszky, G. I. Csonka, O. A. Vydrov, G. E. Scuseria, L. A. Constantin, X. Zhou, and K. Burke, *Phys. Rev. Lett.* **100**, 136406 (2008).
- ³⁷V. I. Anisimov, I. V. Solovyev, M. A. Korotin, M. T. Czyzyk, and G. A. Sawatzky, *Phys. Rev. B* **48**, 16929 (1993); M. T. Czyzyk and G. A. Sawatzky, *ibid.* **49**, 14211 (1994).
- ³⁸L. A. Errico, G. Fabricius, M. Rentería, P. de la Presa, and M. Forker, *Phys. Rev. Lett.* **89**, 055503 (2002); L. A. Errico, G. Fabricius, and M. Rentería, *Phys. Rev. B* **67**, 144104 (2003).
- ³⁹L. A. Terrazos, H. M. Petrilli, M. Marszałek, H. Saitovich, P. R. J. Silva, P. Blaha, and K. Schwarz, *Solid State Commun.* **121**, 525 (2002).
- ⁴⁰P. Blaha, K. Schwarz, and P. H. Dederichs, *Phys. Rev. B* **37**, 2792 (1988); K. Schwarz, C. Ambrosch-Draxl, and P. Blaha, *ibid.* **42**, 2051 (1990).
- ⁴¹L. A. Errico and M. Rentería, *Phys. Rev. B* **73**, 115125 (2006).
- ⁴²H. Haas and J. G. Correia, *Hyperfine Interact.* **198**, 133 (2010).
- ⁴³K. Betsuyaku and H. Harima, *J. Magn. Magn. Mater.* **187-188**, 272 (2004).
- ⁴⁴M. V. Lalic, J. Mestnik-Filho, A. W. Carbonari, R. N. Saxena, and H. Hass, *Phys. Rev. B* **65**, 054405 (2001).
- ⁴⁵E. R. Nieuwenhuis, A. Favrot, Li Kang, M. O. Zacate, and G. S. Collins, *Hyperfine Interact.* **158**, 305 (2004).
- ⁴⁶B. Wodniecka, K. Tomala, P. Wodniecki, M. Marszałek, R. Kmiec and A. Z. Hryniewicz, *Hyperfine Interact.* **110**, 183 (1997).
- ⁴⁷P. Wodniecki, B. Wodniecka, A. Kulińska, and A. Z. Hryniewicz, *J. Alloys Compd.* **264**, 14 (1998).